

Long-term evolution and morphodynamic equilibrium of tidal channels

Stefano Lanzoni

Dipartimento di Ingegneria Idraulica, Marittima e Geotecnica, Università di Padova, Padua, Italy

Giovanni Seminara

Dipartimento di Ingegneria Ambientale, Università di Genova, Genoa, Italy

Received 30 May 2000; revised 25 July 2001; accepted 30 July 2001; published 1 January 2002.

[1] This contribution investigates the morphodynamic equilibrium of funnel-shaped well-mixed estuaries and/or tidal channels. The one-dimensional de Saint Venant and Exner equations are solved numerically for the ideal case of a frictionally dominated estuary consisting of noncohesive sediment and with insignificant intertidal storage of water in tidal flats and salt marshes. This class of estuaries turns out to be invariably flood dominated. The resulting asymmetries in surface elevations and tidal currents lead to a net sediment flux within a tidal cycle which is directed landward. As a consequence, sediments are trapped within the estuary and the bottom profile evolves asymptotically toward an equilibrium configuration, allowing a vanishing net sediment flux everywhere and, in accordance with field observations, a nearly constant value of the maximum flood/ebb speed. Such an equilibrium bed profile is characterized by a concavity increasing as the estuary convergence increases and by a uniquely determined value of the depth at the inlet section. The final length of the estuary is fixed by the longitudinal extension of the very shallow area which tends to form in the landward portion of the estuary. Note that sediment advection is neglected in the analysis, an assumption appropriate to the case of not too fine sediment. *INDEX TERMS:* 4235 Oceanography: General: Estuarine processes, 4558 Oceanography: Physical: Sediment transport, 4255 Oceanography: General: Numerical modeling, 4560 Oceanography: Physical: Surface waves and tides (1255)

1. Introduction

[2] Tidal channels are key features of estuarine and lagoon environments. Quite often they are subject to intense human activity, allowing the development of harbor, shipping channels, and recreational facilities, but they also contain areas of great ecological value which are extremely sensitive to changes caused either by natural factors or human interference. This motivates the increasing attention to the understanding of the complex processes that shape tidal channels, controlling sediment distribution as well as transport of pollutants and biological species.

[3] At the geological time scale, estuaries are fairly recent and ephemeral features. In particular, it has been suggested that estuaries which occupy drowned fluvial valleys (i.e., coastal plain estuaries and rias) and glacial valleys (i.e., fjords and fjards) possibly formed because of the last eustatic and, in geologic terms, rapid rise in sea level of the Flandrian transgression [Perillo, 1995]. Since that time they have gradually adapted to the hydrodynamic conditions typical of each coast, river, and climate in which they have developed. Some evidence also exists suggesting that, at present, many estuaries and coastal lagoons tend toward an equilibrium condition in which the sediment accumulation rate is balanced by the local sea level rise [Stevenson *et al.*, 1986; Nichols, 1989].

[4] In the present contribution we focus our attention on tidal channels or tide-dominated estuaries. Although wave activity and the possible influence of river discharge may become progressively important in the outer and inner portions of the estuary, respectively, tidal currents play a dominant role in controlling

sediment transport. It may be worthwhile to note that even though tide dominance is quite often associated with mesotidal (tidal range 2–4 m) or macrotidal (tidal range >4 m) regimes (e.g., Thames, Gironde, Severn, Coquebid Bay-Salmon, Ord, South Alligator, and Bay of Fundy), it can also occur at smaller microtidal (tidal range <2 m) ranges provided the wave action is limited or the tidal prism is large (e.g., Chesapeake Bay and St. Lawrence Estuary) [Dalrymple *et al.*, 1992]. Indeed, in tide-dominated estuaries the volume of water exchanged by the tide within each tidal cycle is typically at least 1 order of magnitude greater than river discharge.

[5] The morphology of both tidal channels and tide-dominated estuaries is often characterized in plane view by a funnel shape which may be interpreted in terms of an exponential increase of the cross-sectional area toward the mouth (Figure 1). The width to depth ratio of the channel may vary over a large range, attaining values ranging from the order of 10–100 in ria valleys (typical of the northern Spain coast) to 1000 (e.g., Chesapeake Bay). In the seaward portion of the estuarine funnel the bottom morphology is characterized by the presence of a wide variety of bed forms at scales ranging from centimeters to kilometers, tidal sand ridges with superimposed sand waves being the most pronounced morphological features [Dalrymple and Rhodes, 1995]. Intertidal mud flats and marshes flank the landward reach of the estuarine funnel. Progressing up the estuary the funnel shape is typically replaced by an intense meandering channel as the upper limit of the tide influence is approached [Dalrymple *et al.*, 1992].

[6] Sediment dynamics is essentially controlled by the marked distortion and asymmetry of tidal currents which, because of nonlinear effects, develop as the tidal wave propagates from the estuary mouth to the landward reaches of the estuary. Indeed, higher flood velocities having a shorter duration than ebb velocities

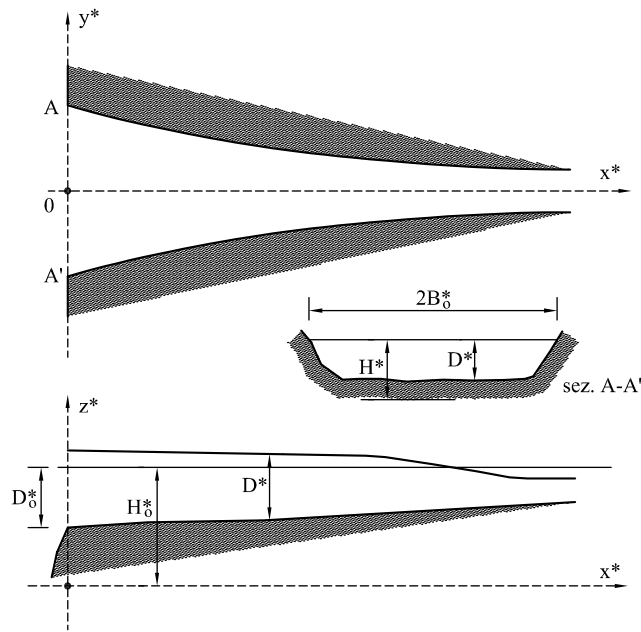


Figure 1. Sketch of the estuary and notations.

and a period of high-water slack longer than that for low-water slack are typical of frictionally dominated, strongly convergent estuaries. They are responsible for the upstream net transport of sand and fine-grained sediment observed in most tide-dominated systems [Wells, 1995]. The material conveyed by littoral transport to the estuary mouth is then moved inside the estuary. In the absence of density-driven circulation, this net landward transport continues to the point where the tide is damped out by frictional attenuation (i.e., the tidal node). Upstream of this point, sediment transport is controlled only by fluvial processes which convey inside the estuary mostly finer sand and mud. However, most of the sediment received from the river ends up being transported and deposited by tidal currents.

[7] The issue that we address in this contribution concerns the possible existence of a long-term longitudinal equilibrium or quasi-equilibrium profile in tide-dominated, well-mixed estuaries. The problem is tackled by formulating a one-dimensional model of both tide propagation and morphodynamic evolution of the tidal channel by coupling the de Saint Venant equations for the flow field and the Exner equation for the bottom evolution. The resulting system is closed by quasi-equilibrium assumptions concerning flow resistance and sediment flux transported as bedload or suspended load. It turns out that on a time scale of hundreds of years an equilibrium may indeed be reached. More precisely, given a tidal input at the mouth of the tidal channel, a width distribution of the channel, and the sediment size, it is shown that the longitudinal bed profile of the channel evolves from an arbitrary initial condition toward some equilibrium configuration characterized by a concavity increasing as the channel convergence increases. The adopted scheme assumes an initial finite length of the channel closed at the inner end and cohesionless sediment. The final equilibrium configuration of the bed profile is characterized by a length determined by the formation of a very shallow area in the inner portion of the channel. Furthermore, the depth at the inlet section is uniquely determined by the final equilibrium state. Finally, the relationship between tidal prism and cross-sectional area in each section of the channel is found to evolve from its initial arbitrary distribution toward a linear relationship of Jarrett's type.

[8] Essentially, our results show that the evolution of the bed profile progressively reduces the initially flood-dominant charac-

ter of tide propagation, though tidal asymmetry persists even in the final equilibrium configuration, until the net flux of sediments throughout a tidal cycle vanishes everywhere in the channel. The somewhat similar idea that progressive infilling of tidal flats and salt marshes could counteract flood dominance, leading to morphodynamic stability, was first suggested by *Boon and Byrne* [1981]. On the contrary, *Friedrichs and Aubrey* [1988], on the basis of numerical experiments based on *Speer and Aubrey's* [1985] one-dimensional model of tide propagation in trapezoidal channels with constant depth and fixed bed, had concluded that infilling of tidal channels characterized by flood dominance (without an increase of intertidal area) should only enhance the flood dominant character of the channel. Such a conclusion does not contradict the present results as the evolution of the bed profile, hence of channel geometry, is responsible for the evolution of the tidal wave. Related work has also been performed by a Dutch group in Utrecht [*Schuttelaars and de Swart*, 1996, 2000]. Since such work tackles a problem similar to the present one, a detailed discussion of their approach is presented in section 5.

[9] The rest of the paper is organized as follows. In section 2 the hydrodynamic problem of tide propagation in a convergent tidal channel is formulated. Section 3 is devoted to the formulation of the morphodynamic problem. Section 4 discusses the numerical approach employed to solve the governing equations. Finally, section 5 describes the main results along with some concluding remarks.

2. Hydrodynamic Problem

[10] Let us consider a tidal channel of length L_e^* and average flow depth D_0^* at the mouth (hereafter a star apex will denote dimensional quantities). Also, let B^* denote the effective width of the cross section, defined as the width of an equivalent rectangular cross section. The width B^* is assumed to vary along the landward oriented longitudinal axis x^* according to a classical exponential law, namely,

$$B^* = B_0^* \exp\left(\frac{-x^*}{L_b^*}\right), \quad (1)$$

where B_0^* is the width at the mouth and L_b^* will be called convergence length (see Figure 1). In the following, as a first step in the analysis, we neglect the possible presence of tidal flats flanking the main channel. The effect of these adjacent wetlands, however, can be accounted for by suitably modifying the continuity equation [*Speer and Aubrey*, 1985; *Jay*, 1991; *Shetye and Gouveya*, 1992].

[11] The basic one-dimensional partial differential equations describing the unsteady water flow in a wide rectangular channel are the classical shallow water equations of mass and momentum conservation, which read

$$B^* D_{,t^*} + (B^* D^* U^*)_{,x^*} = 0 \quad (2)$$

$$U^*_{,t^*} + U^* U^*_{,x^*} + g H^*_{,x^*} + \frac{U^* |U^*|}{C^2 D^*} = 0, \quad (3)$$

where t^* denotes time, D^* is the local flow depth, H^* is water surface elevation, U^* is local depth-averaged velocity, g is gravity, and C is flow conductance which can be estimated on the basis of bed material and bed form characteristics [e.g., *van Rijn*, 1990].

[12] Denoting by ω^* , D_0^* , U_0^* , and C_0 , the angular frequency of the main component of the tidal wave, a typical value of the depth-averaged flow velocity, and a characteristic flow conductance,

respectively, the relevant variables of the problem are made dimensionless as follows:

$$t^* = \omega^{*-1} t \quad (D^*, H^*) = D_0^*(D, H); \quad U^* = U_0^* U; \quad C = C_0 C. \quad (4)$$

As regards to the longitudinal coordinate x^* , we make it dimensionless by employing an a priori unknown scale L_0^* . The actual value of L_0^* will vary depending on the dominant balance prevailing in the momentum equation for each particular tidal flow. The resulting dimensionless form of (2) and (3) then read [Lanzoni and Seminara, 1998]

$$\frac{1}{\epsilon} D_{,t} + \mathcal{F}(UD)_{,x} - \mathcal{K}UD = 0, \quad (5)$$

$$SU_{,t} + \epsilon S\mathcal{F}UU_{,x} + \frac{1}{\epsilon} H_{,x} + \mathcal{R} \frac{U|U|}{C^2 D} = 0, \quad (6)$$

where the following dimensionless parameters arise:

$$\epsilon = \frac{a_0^*}{D_0^*}; \quad \mathcal{F} = \frac{1}{\epsilon} \frac{U_0^*}{\omega^* L_0^*}; \quad \mathcal{K} = \frac{1}{\epsilon} \frac{U_0^*}{\omega^* L_b^*}; \quad (7)$$

$$S = \frac{F_0^2 \omega^* L_0^*}{\epsilon U_0^*}; \quad \mathcal{R} = \frac{F_0^2}{\epsilon} \frac{L_0^*}{C_0^2 D_0^*}. \quad (8)$$

Here $F_0 = U_0^*/(gD_0^*)^{1/2}$ denotes the flow Froude number, C_0 is a typical value of the average flow conductance coefficient, and a_0^* is the amplitude of the tidal wave at the estuary mouth. Note that the factor in the last term of (6) allows one to account for spatial and temporal variations of flow conductance caused by changes in bed form characteristics during the tidal cycle.

[13] The parameter \mathcal{K} in the continuity equation (5) is a relative measure of the degree of width convergence of the estuary; the parameters S and \mathcal{R} in the momentum equation (6) weight the relative importance of local acceleration and friction, respectively, with respect to gravity; and finally, the parameter is related to the spatial variations of flow discharge associated with depth and velocity changes. Four limiting cases exist depending on the values attained by \mathcal{K} and by the ratio \mathcal{R}/S , namely, weakly convergent ($\mathcal{K} \ll 1$) and weakly dissipative ($\mathcal{R}/S \ll 1$) estuaries, weakly convergent and strongly dissipative ($\mathcal{R}/S = O(1)$) estuaries, strongly convergent ($\mathcal{K} = O(1)$) and weakly dissipative estuaries, and strongly convergent and strongly dissipative estuaries. Lanzoni and Seminara [1998] calculated the values attained by \mathcal{K} and \mathcal{R}/S in numerous estuaries, showing that a high degree of convergence and a predominance of friction over local inertia are distinctive features of a wide class of estuaries. These estuaries are found to be invariably flood dominated, provided the effect of tidal flats and salt marshes flanking the main estuarine channel is not too large. Conversely, estuaries characterized by relatively large flow depths (and therefore weak friction) and extensive regions of flats and marshes are usually ebb dominated [Friedrichs and Aubrey, 1988; Speer et al., 1991; Lanzoni and Seminara, 1998].

[14] The boundary condition at the estuary mouth is given by the sea level fluctuation. Although the various tidal constituents typically present could be easily accounted for, many features of estuarine channel response to tidal forcing are revealed by concentrating our attention on the first harmonic M_2 [Speer and Aubrey, 1985; Parker, 1991]. We then assume that the dimensionless flow depth at the channel mouth varies according to the law

$$D|_{x=0} = 1 + \epsilon \cos(t). \quad (9)$$

At the landward boundary we assume a condition suitable for tidal channels in coastal lagoons, which, at the inner end, shoal to

depths less than the offshore average tidal amplitude. Hence we set

$$U|_{x=0} = 0. \quad (10)$$

This boundary condition is also suitable for tide-dominated estuaries characterized by negligible freshwater discharge supply.

[15] The hydrodynamic problem (equations (5), (6), (9), (10)) is immediately seen to be coupled with the morphodynamic problem if one recognizes that the flow depth D^* reads

$$D^* = H^* - \eta^*, \quad (11)$$

with η^* being the average bottom elevation at each cross section. We now complete our formulation by addressing the morphodynamic problem for η^* .

3. Morphodynamic Problem

[16] Several factors contribute to determine the sediment balance in a tidal channel, namely, (1) channel geometry, i.e., the degree of convergence of the channel induced both by its funnel planimetric shape and by the sloping character of the bed and the degree of channel sinuosity, which controls the hydrodynamics of tide propagation along the channel; (2) the harmonic content of the tidal oscillation acting at the inlet; (3) the fluvial transport of sediment discharged by the river at the upstream end of the estuary; and (4) the lateral exchange of sediments between the channel and the adjacent tidal flats. In the present contribution, only factor 1 was examined, considering a straight, convergent channel closed at one end and connected at the other end with a tidal sea characterized by a tidal oscillation consisting of a single harmonic. The possible presence of tidal flats was ignored.

[17] Estuarine sediments are derived both from fluvial and marine sources, the grain sizes ranging from sands to mud. In tide-dominated estuaries a dominance of sand is typically found in channels, whereas a dominance of silt and clay characterizes the adjacent tidal flats and/or salt marsh deposits [Wells, 1995].

[18] Coarser sand particles (usually derived from the continental shelf or from the erosion of the shoreline) are transported as bed load when current speed exceeds a well-defined threshold in either the flood or ebb directions. Such a threshold is usually given in terms of the critical value θ_c of a dimensionless form of the average shear stress τ_0^* acting on the bed, called Shields stress, defined as

$$\theta = \frac{\tau_0^*}{(\rho_s - \rho)gd_s^*} = \frac{u_*^2}{\Delta gd_s^*}, \quad (12)$$

where $u_* (=U^*/C)$ is the average friction velocity, ρ and ρ_s are water and particle density, respectively, $\Delta = \rho_s/\rho - 1$, d_s^* is average particle diameter, and g is gravity. More specifically, bed load occurs for values of θ exceeding θ_c but lower than a second threshold value θ_{cs} , depending on the particle Reynolds number $R_p t(\sqrt{\Delta g d_s^{*3}}/\nu)$, with ν kinematic viscosity of water), which defines the threshold condition for entrainment in suspension [Bagnold, 1966; Engelund, 1965; van Rijn, 1984b].

[19] The magnitude and direction of the net transport over a tidal cycle is thus mainly affected by tidal asymmetries favoring unequal duration and/or unequal magnitude of ebb and flood [Dronkers, 1986]. In particular, flow asymmetries characterized by shorter flood duration and higher flood current maximum (i.e., flood dominance) induce a landward directed sediment transport. Conversely, shorter fall periods and greater ebb current maxima (ebb dominance) cause a net seaward directed sediment transport.

[20] Fine sand particles, silt, and clay (normally of fluvial origin) are carried into suspension whenever upward grain movement induced by vertical turbulent bursts exceeds gravitational settling in the suspending fluid [Sumer and Deigaard, 1981; Niño

and Garcia, 1996]. Sediment suspension then requires that the current speed exceeds a critical value such that the Shields stress θ is over the threshold θ_{cs} defined above. Therefore in asymmetrical currents, suspended load can take place for different time intervals in the various phases of the tidal cycle. Moreover, in unsteady flows the continuous adjustment of the sediment transport to the sediment transport capacity yields both a scour and a settling phase lag. Hence the amount of suspended sediment and the time variations of the vertical distribution of concentration may be significantly affected by the asymmetries in flow acceleration during the two slack water intervals centered on slack before flood and slack before ebb [Nichols and Boon, 1994; Dyer, 1995].

[21] In the present contribution, as a first step, the bottom of the estuary is assumed to consist of cohesionless, nearly uniform sediment which may be transported either as bed load or as suspended load, depending on the value of the bottom shear stress. Both bed load and suspended load are assumed to adapt instantaneously to local flow conditions. We thus neglect scour and settling lag effects which, especially in tidal flats, may contribute appreciably to the residual flux of muddy sediments [Postma, 1961; Groen, 1967]. The physical basis of this assumption is discussed later. Here we note that a large number of field observations suggest that in estuarine channels the adjustment of suspended sediment concentration to changes in bottom shear stress is extremely rapid [Allen et al., 1980; Officer, 1981; van Rijn, 1990].

[22] Sediment continuity requires that the following differential equation [Exner, 1925] be satisfied:

$$(1-p)B^*\eta_{1,x^*} + (B^*q_s^*)_{,x^*} = 0, \quad (13)$$

where p is sediment porosity, q_s^* is the total sediment flux per unit width, and we have neglected the effect of local variation of the cross-sectionally averaged sediment concentration. The latter equation simply states that spatial variations of the total sediment flux $B^*q_s^*$ lead either to bed aggradation or bed degradation. Hence in a tidal environment an exact morphodynamic equilibrium cannot exist. However, an average equilibrium (the average being referred to the tidal cycle) may indeed be reached provided the average sediment flux over a tidal cycle vanishes everywhere along the channel. Such equilibrium may be attained through a slow adjustment of the bed profile which, affecting tide propagation, modifies the stress field and hence the sediment flux. Morphodynamics and hydrodynamics are then strictly coupled in such a long-term evolution process. Exner's sediment balance equation can be put in the following dimensionless form:

$$\eta_{,\tau} + \left(q_{s,x} - \frac{\mathcal{K}}{\mathcal{F}} q_s \right) = 0, \quad (14)$$

where

$$t^* = T_0^* \tau; \quad \eta^* = D_0^* \eta; \quad q_s^* = \sqrt{\Delta g d_s^{*3}} q_s; \quad T_0^* = \frac{(1-p)D_0^* L_0^*}{\sqrt{\Delta g d_s^{*3}}} \quad (15)$$

with T_0^* the typical morphological time scale.

[23] In order to complete the formulation we need closure relationships for the total amount of sediment flux per unit width q_s^* instantaneously transported by the tidal current at a given location, calculated as the sum of bed load flux per unit width q_{sb}^* and the suspended load flux per unit width q_{ss}^* . Providing such closure relationships is a formidable task which still awaits the development of fully satisfactory, theoretically well-founded tools. In spite of such relative uncertainty, a few fairly well-established results of semiempirical nature have been widely employed in the literature. They refer to the simplest flow conditions, namely, uniform free surface flow on a homogeneous cohesionless bed, a configuration that by definition is in equilibrium, i.e., such that the elevation of the bed interface keeps constant in time.

[24] Various relationships have been proposed in the literature to quantify the bed load transport rate in rivers [e.g., Meyer-Peter and Müller, 1948; van Rijn, 1984a]. All these formulas have been derived on the basis of unidirectional flow data. The question then arises whether the above formulations are appropriate also to tidal environments where flow unsteadiness may, in principle, lead to nonequilibrium effects. Quantifying these effects in the context of one-dimensional models is a fairly unexplored subject which will require attention in the near future. In the present contribution we neglect nonequilibrium effects and estimate the bed load flux per unit width by employing the equilibrium formula of Meyer-Peter and Müller [1948] which has already been used successfully in nearshore applications [Goud and Aubrey, 1985]. It reads

$$q_{sb}^* = 8(\theta - \theta_c)^{3/2} \sqrt{\Delta g d_s^{*3}}. \quad (16)$$

[25] As far as suspended load is concerned, the flow conditions for initiation of suspension were evaluated on the basis of the criterion proposed by Bagnold [1966] stating that suspension takes place when the value of the friction velocity u^* equals the particle fall velocity w_s^* . Bagnold's condition has been applied herein to the local and instantaneous flow conditions. In a one-dimensional formulation, in order to evaluate the suspended load flux per unit width q_{ss}^* one would strictly need to evaluate the spatial and temporal distribution of the local concentration of suspended sediment averaged over turbulence $\langle c \rangle$. More specifically, we have

$$q_{ss}^* = \sqrt{\Delta g d_s^{*3}} q_{ss} = \frac{1}{B^*} \int_{-B^*/2}^{B^*/2} dy^* \int_{\eta^*}^{H^*} (\langle c \rangle \langle u^* \rangle + \langle c' u'^* \rangle) dz^*, \quad (17)$$

where y^* and z^* are the transverse and vertical axis, respectively (see Figure 1); c and u^* are the local and instantaneous values of the sediment concentration and of the longitudinal component of the velocity vector, respectively; c' and u'^* are the fluctuating components of the Reynolds decomposition of c and u^* , respectively; and $\langle \dots \rangle$ denotes average over turbulence.

[26] The effect of advective transport of suspended sediment on $\langle c \rangle$ was accounted for by Friedrichs et al. [1998], who suggest its importance, though in the context of a linearized treatment of the frictional term in the momentum equation. Nevertheless, a simple scaling argument [Galappatti, 1983; Galappatti and Vreugdenhil, 1985] shows that, at the leading order of approximation in an expansion in powers of suitable parameters, q_{ss}^* can be simply evaluated using relationships established for the case of transport in suspension in uniform turbulent-free surface flows, i.e., resorting to the classical Rouse [1937] solution. In fact, denoting by w^* the local and instantaneous value of the vertical component of the velocity vector; by W_0^* a typical value of w^* ; by \mathcal{D}_T^* the eddy diffusivity, a quantity which several experimental investigations suggest to attain values slightly different from the corresponding values of the eddy viscosity; by $u_0^* (= U_0^*/C_0)$ a typical value of the friction velocity; and introducing the scaling

$$\langle \langle u^* \rangle, \langle w^* \rangle \rangle = (U_0^* \langle u \rangle, W_0^* \langle w \rangle); \quad z^* = D_0^* z; \quad \mathcal{D}_T^* = u_{*0} D_0^* \mathcal{D}_T, \quad (18)$$

the convection-diffusion equation for plane flows in dimensionless form reads

$$\delta_1 \frac{\partial \langle c \rangle}{\partial t} + \delta_2 \langle u \rangle \frac{\partial \langle c \rangle}{\partial x} + \delta_3 \langle w \rangle \frac{\partial \langle c \rangle}{\partial z} - kZ_0 \frac{\partial \langle c \rangle}{\partial z} = \frac{\partial}{\partial z} \left(\mathcal{D}_T \frac{\partial \langle c \rangle}{\partial z} \right) + \delta_4 \frac{\partial}{\partial x} \left(\mathcal{D}_T \frac{\partial \langle c \rangle}{\partial x} \right), \quad (19)$$

where k is the von Karman constant; $Z_0(=w_s^*/ku_{*0})$ is a characteristic value of the so-called Rouse number, which controls the vertical distribution of concentration; and the following dimensionless parameters arise:

$$\delta_1 = \frac{\omega^* D_0^*}{u_{*0}} \quad \delta_2 = \frac{U_0^* D_0^*}{u_{*0} L_0^*} \quad \delta_3 = \frac{W_0^*}{u_{*0}} \quad \delta_4 = \frac{D_0^{*2}}{L_0^{*2}}. \quad (20)$$

[27] Simple estimates immediately suggest that the parameters Z_0 and \mathcal{D}_T are $O(1)$ quantities, while the parameters δ_1 and δ_4 are definitely small. In fact, with ω^* , D_0^* , and u_{*0} ranging about 1.4×10^{-4} , 10 m, and 5 cm s^{-1} , respectively, one finds that δ_1 ranges about 0.028. On the other hand, with L_0^* of the order of kilometers, δ_4 is of order 10^{-3} . Finally, since the vertical velocity associated with tide propagation may reach, at most, a fraction of mm s^{-1} , the parameter δ_3 is also at most of order 10^{-2} . More delicate is the role of the longitudinal advective term; in fact, with U_0^* ranging about 1 m s^{-1} and D_0^*/L_0^* of order 10^{-2} , the parameter δ_2 would range about 0.2. The above arguments, which were first put forward by Galappatti [1983], suggest that the solution for $\langle c \rangle$ can be expanded in powers of the small parameter δ_2 possibly including the effects of vertical convection, longitudinal turbulent diffusion, and local variations of mean concentration once suitable relationships are established among the various small parameters appearing in (20). At the leading order of approximation, (19) reduces to the classical uniform balance between vertical depositing flux associated with the settling speed and the mean upward vertical flux associated with turbulent diffusion. In the present work we have restricted our analysis to such approximation, which allows us to calculate the mean total sediment flux by means of classical relationships [e.g., Engelund and Hansen, 1967; van Rijn, 1984b] established for uniform free surface flows, evaluated in terms of the local instantaneous conditions determined at each cross section by tide propagation. In fact, our aim was to ascertain whether equilibrium may be achieved in the presence of leading order effects. The analysis of additional effects, in particular sediment advection, will be pursued in further developments of the present work.

[28] The flux of suspended sediment then was calculated employing the classical vertical distribution of sediment concentration associated with the local and instantaneous characteristics of the flow field. The resulting expression for q_{ss}^* , written in the form of van Rijn [1984b], reads

$$q_{ss}^* = \mathcal{L} U^* D^* c_a, \quad (21)$$

where c_a is a reference concentration at the height a^* above the bed and the dimensionless shape factor \mathcal{L} can be satisfactorily approximated by the following relationship:

$$\mathcal{L} = \frac{\zeta^Z - \zeta^{1.2}}{(1 - \zeta)^Z (1.2 - Z)}.$$

Here $\zeta = a^*/D^*$ and $Z = w_s^*/(ku_{*0})$ is the Rouse number. Empirical relationships for c_a and a^* have been proposed by various authors. Herein we follow van Rijn [1984b] and write

$$c_a = 0.015 \frac{d_{50}^* T^{1.5}}{a^* R_p^{0.2}} \quad (22)$$

$$a^* = \begin{cases} e_r^* & (e_r^* \geq 0.01 D^*) \\ 0.01 D^* & (e_r^* < 0.01 D^*), \end{cases} \quad (23)$$

where d_{50}^* is the grain size such that 50% of the sediment is finer, $T = (\theta' - \theta_c)/\theta_c$ is a transport stage parameter, θ' is the Shields parameter based on the grain roughness flow conductance C_r

($= 2.5 \ln 4 D^*/d_{90}^*$), and R_p is the particle Reynolds number previously defined. The overall bed roughness height e_r^* generally depends on the presence of small-scale bed forms on the bed and can be estimated by means of the following relationship:

$$\epsilon \epsilon_r^* = 3d_{90}^* \quad e_r^* = 3d_{90}^* \quad (T \geq 25) \\ \epsilon \epsilon_r^* = 3d_{90}^* + 1.1 A^* [1 - \exp(-25 A^*/L^*)] \quad (0 < T < 25), \quad (24)$$

where d_{90}^* is the grain size such that 90% of the sediment is finer and A^* and L^* are dune amplitude and wavelength, respectively, given in the form

$$L^* = 7.3 D^* \\ A^* = 0.11 D^* (d_{50}^*/D^*)^{0.3} [1 - \exp(-T/2)] (25 - T). \quad (25)$$

Note that within a neighborhood of the instant of flow reversal, no bed load transport occurs, as θ does not exceed θ_c . Similarly, when θ falls below the threshold value θ_{cs} for particle entrainment in suspension, only sediment deposition occurs. However, such an effect cannot be included in the context of a one-dimensional model, requiring a detailed evaluation of the temporal evolution of the concentration profile close to flow reversal. In the present contribution, given the already heavy computational effort required to perform long-term predictions, we will neglect the latter effect. Further developments will be required to ascertain how severe the latter approximation is.

[29] The formulation of the morphodynamic problem is completed by imposing that the instantaneous sediment flux at the inner end of the channel must vanish. This condition is automatically satisfied having imposed that the instantaneous cross-sectionally averaged speed must also vanish at the inner boundary (see (10)).

4. Numerical Approach

[30] The solution of the complete unsteady equations for the liquid phase (5) and (6) and solid phase (14), except for very simple idealized cases where the governing equations are heavily simplified [e.g., Schuttelaars and de Swart, 1996, 2000], must be obtained numerically. In many practical applications the one-dimensional simulation of unsteady sediment transport can be carried out by decoupling the solution for the fluid phase from that governing the bed evolution at each time step [see Cunge *et al.*, 1980]. Indeed, the morphologic time scale T_0^* on which the bottom evolves is typically a few orders of magnitude larger than the hydrodynamic time scale $2\pi/\omega^*$, thus ensuring that the flow fields adapt nearly instantaneously to changes in the bottom configuration. Nevertheless, as explained by Lyn [1987], for problems in which changes in both fluid and sediment discharge imposed at the boundaries are relatively fast compared with the time scale of changes in bed elevation, a model in which hydraulic and sediment variables are coupled is indeed necessary [see also Lyn and Goodwin, 1987].

[31] In order to avoid the possible growth of parasitic oscillations in bed elevation arising from the singularly perturbed nature of movable-bed problems, the numerical solution of (5), (6), and (14) was carried out by using the two-step predictor-corrector explicit finite difference scheme of MacCormack which, owing to the predictor-corrector approach, ensures the coupling of flow equations and sediment continuity equation. Furthermore, it allows us to handle shocks and discontinuities without any special treatment, provided that the differential equations are written in conservative form [see Hirsch, 1990a, p. 237] and a suitable artificial viscosity is introduced in order to remove the unavoidable high-frequency oscillations around discontinuities typical of second-order central schemes.

[32] The details of the adopted numerical algorithm and of the computational procedure are given by Bhallamudi and Chaudhry

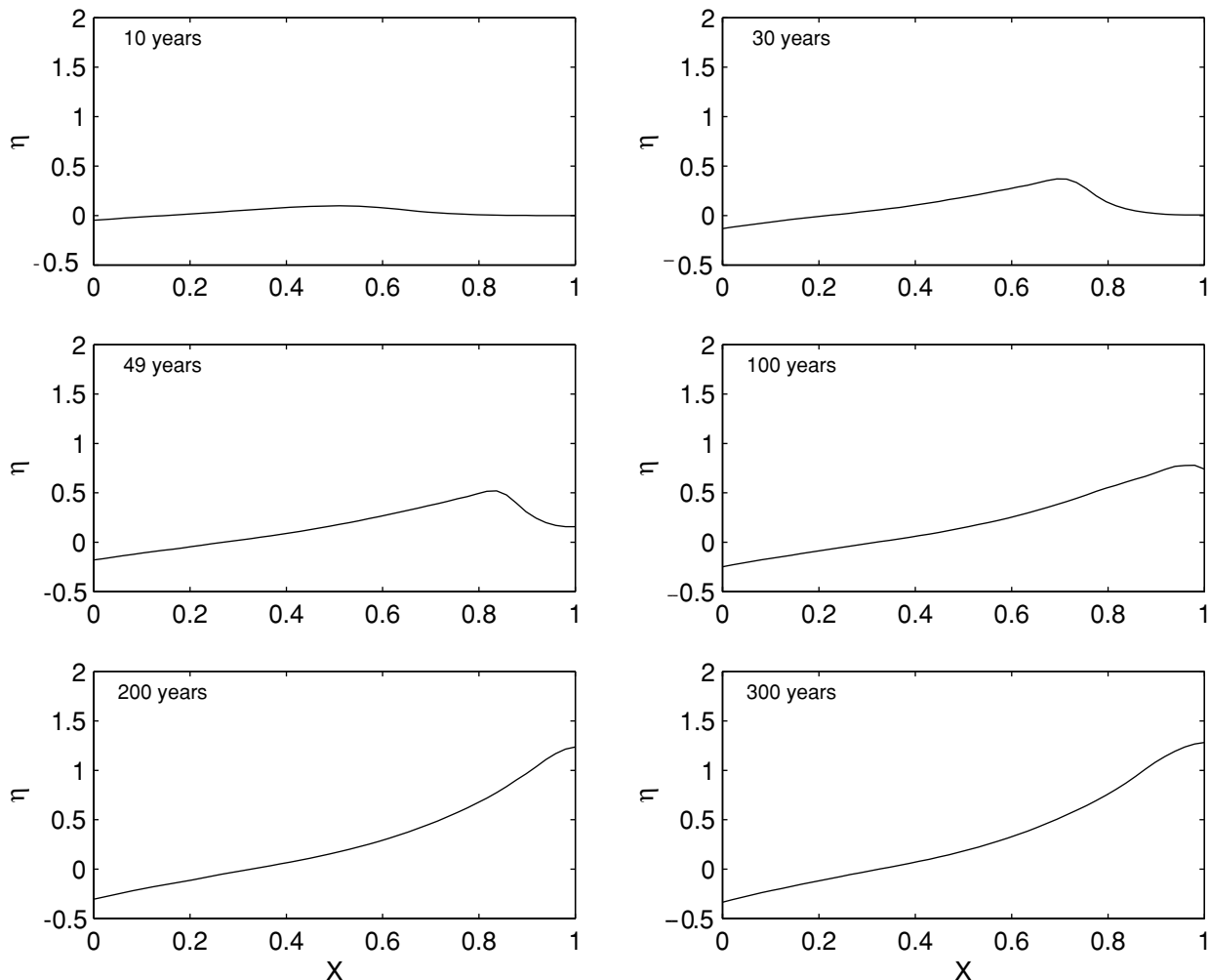


Figure 2. Example of the temporal evolution of the bottom profile from an initially plane configuration for a strongly convergent, strongly dissipative estuary. The bottom elevation at each cross section has been scaled with the initially uniform depth D_0^* (i.e., $\eta = \eta^*/D_0^*$), while the estuary length L_e^* has been used to scale the longitudinal coordinate (i.e., $X = x^*/L_e^*$). The values of the relevant dimensionless parameters adopted in the calculation are: $\beta = 0.16$, $\mathcal{K} = 0.60$, $\mathcal{S} = 0.34$, $\mathcal{R} = 1.0$, $\epsilon = 0.29$, and $d_s = d_s^*/D_0^* = 1.33 \times 10^{-5}$. These values, for example, can be achieved by considering an estuary 30 km long, with a convergence length of 25 km, an initial depth of 7.5 m, and a mean sediment grain diameter of 0.1 mm, forced by a semidiurnal tide with amplitude 2.2 m, characterized by a velocity scale $U_0 = 0.6 \text{ m s}^{-1}$, and a Manning roughness coefficient of $0.0326 \text{ s m}^{-1/3}$.

[1991]. Here we only note that in the predictor step the spatial derivatives are approximated by forward first-order finite differences, while in the corrector step they are approximated by backward first-order finite differences, using the predicted variables. As far as the variables at the boundary are concerned, the predictor forward step was used to estimate the predictor values of water speed and bottom elevation at the mouth of the estuary; the corrector backward step allowed us to calculate the corrector values of both water and bed elevations at the landward end of the estuary. In order to obtain global boundary values, the predictor values of water and bottom elevations at the landward boundary were specified by a zero-order time extrapolation [see *Hirsch*, 1990b, p. 353]; the corrector values of water speed and bed elevation at the estuary mouth, on the other hand, were calculated using a first-order space extrapolation. As will be discussed in section 5, the morphological evolution of the estuary is characterized by the formation of a sediment front which migrates landward. As this discontinuous front reaches the inner end of the estuary and until it is completely reflected, the above procedure

employed to estimate the predictor and corrector values of bed elevation at the landward boundary must be temporarily modified. The bottom elevation is then estimated on the basis of an integral (i.e., weak) formulation of the sediment balance equation which allows us to write the relationship between bottom elevations and sediment fluxes on both sides of the sediment front [see *Abbott*, 1974; *Garcia-Navarro and Saviron*, 1992].

[33] A further problem encountered in the simulations was related to the need for reproducing the repetitive flooding and drying of the very shallow area which, as a consequence of the morphological evolution of the bottom, tends to form close to the landward end of the estuary. Note that such a shoaling portion of the estuary is distinct from the intertidal storage areas which are ignored in the present analysis. Various numerical techniques have been proposed to cope with wetting and drying problems: A wide review on this subject is given by *Bates and Hervouet* [1999]. Here we follow the approach proposed by *Defina* [2000] [see also *Defina et al.*, 1994] according to which the differential equations governing the

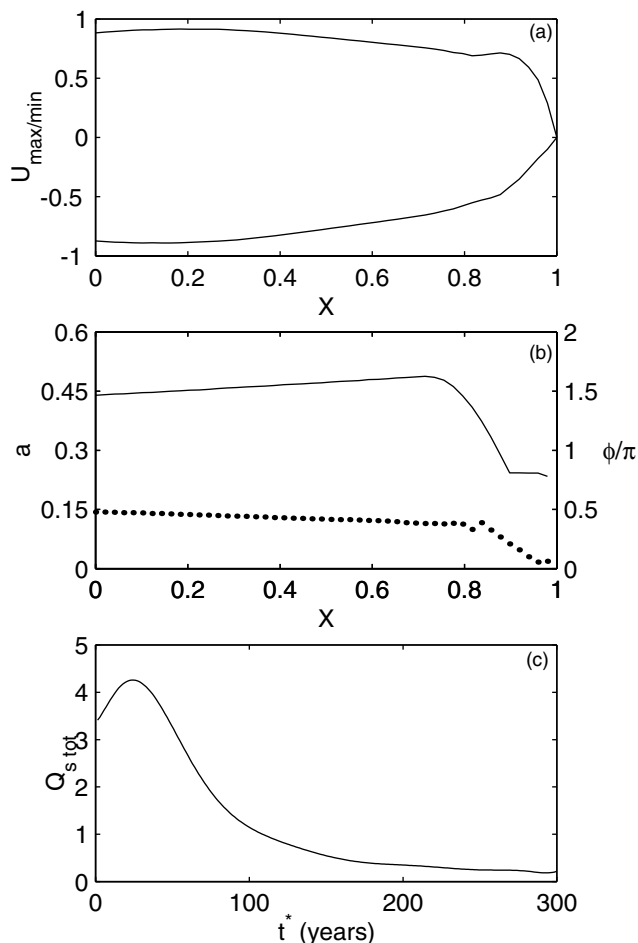


Figure 3. (a) Maximum dimensionless flood/ebb flow speed (scaled with U_0^* , i.e., a typical value of the depth-averaged velocity within the estuary) and (b) dimensionless tidal amplitude a (scaled with the value of the flow depth at the outlet) and phase lag ϕ between the maximum tide elevation and the maximum flood flow speed plotted along the estuary for the final bottom configuration shown in Figure 2. The estuary length L_c^* has been used to scale the longitudinal coordinate (i.e., $X = x^*/L_c^*$). (c) Temporal evolution of the global dimensionless net sediment flux Q_{stot} (i.e., tidally averaged, integrated all along the estuary, and scaled by $\sqrt{\Delta g d_s^3}$) for the bottom evolution shown in Figure 2.

flow over partially wet elements are reformulated by introducing a subgrid model based on the statistics of bottom topography, thus allowing for the application of classical numerical schemes without any special modification. A brief description of the procedure proposed by Defina [2000] to obtain the set of shallow water equations for partially wet domains is reported in Appendix A, where such a procedure is also employed to obtain a suitable form of the sediment fluxes to be used in the sediment balance equation.

5. Discussion and Results

[34] Estuaries and coastal lagoons, which may be regarded as ephemeral landforms at the geological time scale, have been shown in the present work to be able to reach a morphodynamic equilibrium (or quasi-equilibrium) on much shorter time scales, of the order of hundreds of years. Strictly speaking, (14) implies that an equilibrium configuration (i.e., $\eta_{,\tau} = 0$) is attained if the net

sediment flux (i.e., averaged over a tidal cycle and hereafter denoted by an overbar) either vanishes everywhere or increases landward according to the relationship

$$\bar{q}_s = \bar{q}_{s0} \exp\left(\frac{\mathcal{K}}{\mathcal{F}}x\right). \quad (26)$$

However, the latter equilibrium requires sediment entering and/or leaving the estuary at the seaward and landward boundaries. In the case treated in the present paper, where at the landward boundary we have assumed the existence of an impermeable barrier (or, alternatively, of a shoaling bottom) equilibrium is only achieved provided $\bar{q}_s = 0$. Also, note that a zero net sediment flux does not necessarily imply a vanishing sediment discharge at every instant of the tidal cycle, hence it does not prevent the development and migration of tidal bed forms.

[35] Before discussing in detail the present results, it may be worthwhile to review the theoretical work carried out by *Schuttelaars and de Swart* [1996, 2000] which treated a problem similar to the one formulated in sections 2 and 3. The approach employed by the latter authors differs from our approach in several respects. In particular, *Schuttelaars and de Swart* [1996] restrict themselves to the case of “short” idealized tidal embayments, consisting of rectangular channels with constant width (no convergence, no tidal flats) closed at one end (no river discharge) and connected at the mouth with a tidal sea. Because of the short length of the channel the free surface oscillation was affected neither by inertia nor by friction; in other words, at the leading order of approximation, free surface oscillations were found to be spatially uniform. Flow continuity then gives the velocity distribution in terms of the unknown spatial distribution of flow depth. The latter should arise from the constraint that the net sediment flux in a tidal cycle must vanish. However, at the leading order of approximation the latter constraint is identically satisfied for any spatial distribution of flow depth. *Schuttelaars and de Swart* [1996] overcame such difficulty by arbitrarily assuming that such distribution was linear. Various other approximations were introduced. In particular, a depth-integrated form of the convection-diffusion equation for the concentration was employed where the contributions associated with the local temporal variation of mean concentration and the longitudinal diffusive contribution were retained, while the longitudinal advective contribution was neglected. The scaling argument of *Galappatti* [1983] reproduced in section 3 does not seem to substantiate such procedure. Moreover, the frictional term was linearized, a procedure which can indeed be justified in relatively short tidal embayments where such contribution would affect the net sediment flux only at a higher order of approximation [*Lanzoni and Seminara*, 1998]. More recently, *Schuttelaars and de Swart* [2000] extended their previous work to the case of tidal embayments of arbitrary lengths. Various approximations were similar to those employed in the previous work. In particular, friction was linearized, an approximation which may produce undue steepening of the tidal wave in strongly dissipative estuaries, as shown by *Lanzoni and Seminara* [1998], and fails completely when the flow depth tends to vanish, as it occurs in the drying and wetting portion of the flow domain. This difficulty was, indeed, recognized by *Schuttelaars and de Swart* [2000], who employed an artificial procedure to circumvent it. Unlike the present work, *Schuttelaars and de Swart* [2000] did not describe the wetting and drying portion of the flow domain and simply imposed their landward conditions at a fixed boundary where an artificial hydrodynamic condition, described as “kinematic condition,” is imposed. Furthermore, *Schuttelaars and de Swart* [2000] force the bottom elevation at the channel mouth to keep artificially constant, unlike the present work where the bottom profile evolves in time until it reaches its equilibrium configuration everywhere in the channel, including the inlet. We wonder whether the latter constraint was the cause of the peculiar bed profiles obtained by *Schuttelaars and*

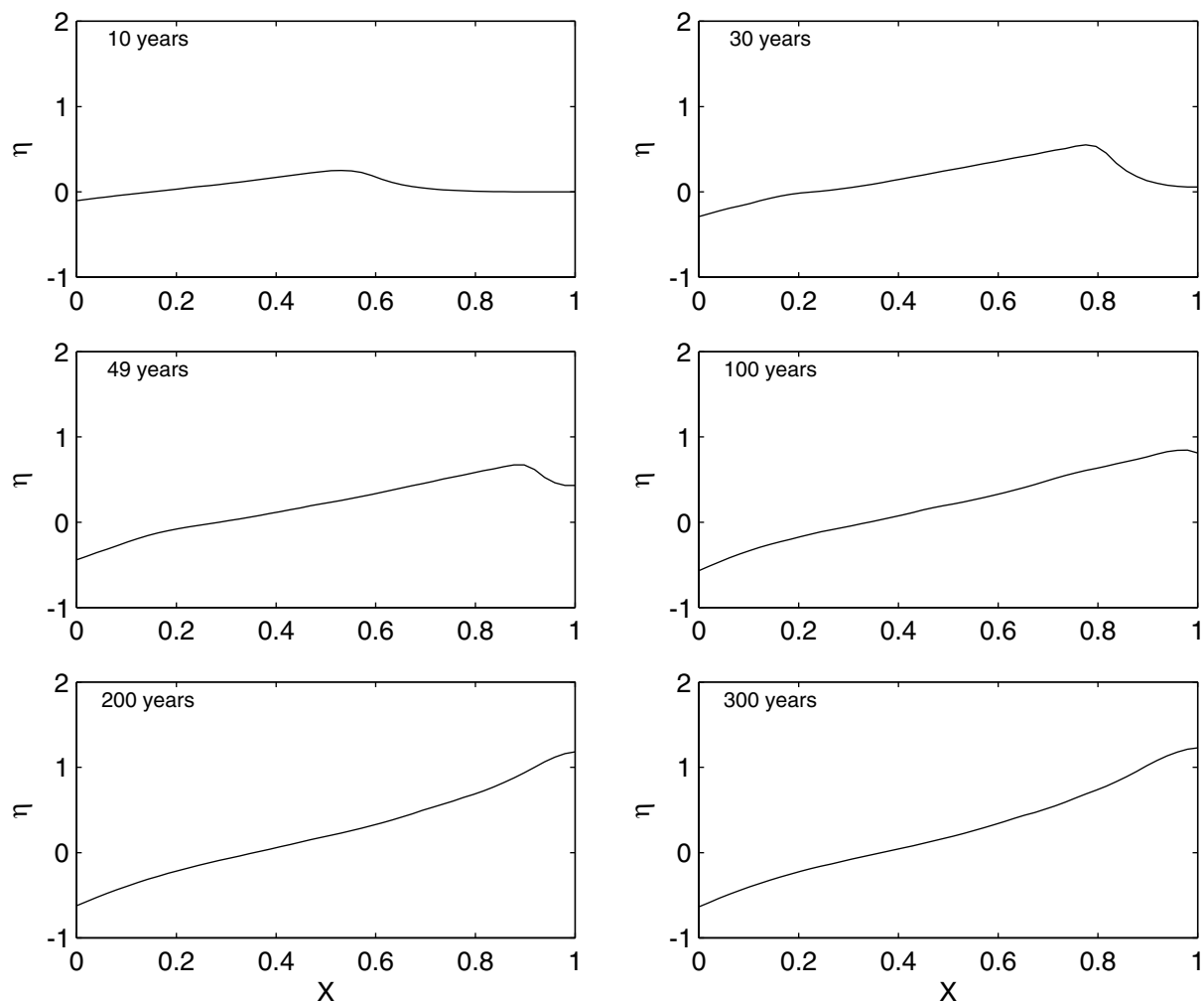


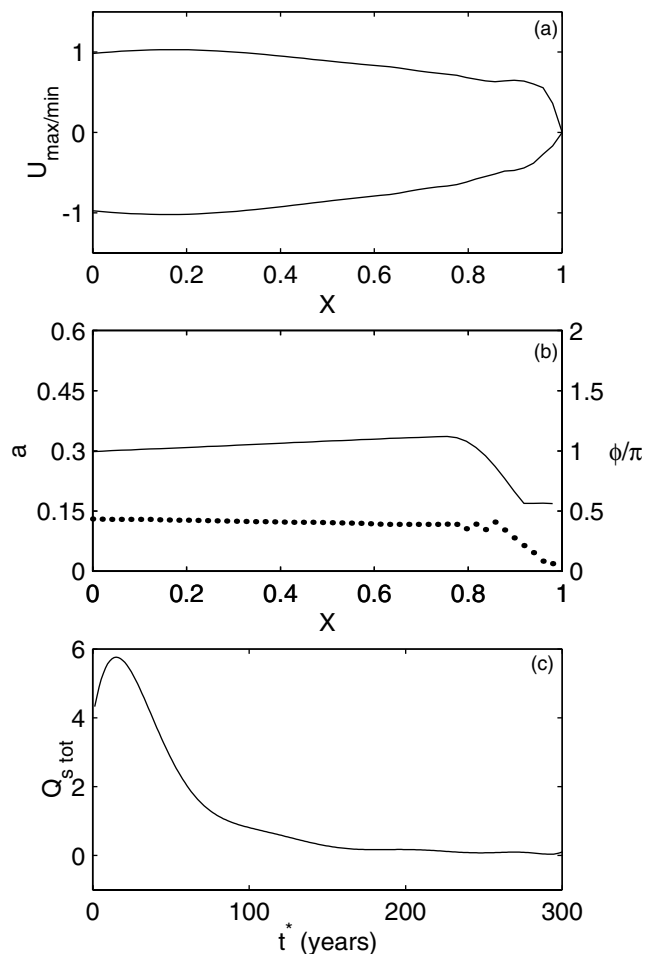
Figure 4. Example of the temporal evolution of the bottom profile from an initially plane configuration for a strongly dissipative estuary of constant width. The bottom elevation at each cross section has been scaled with the initially uniform depth D_0^* (i.e., $\eta = \eta^*/D_0^*$), while the estuary length L_e^* has been used to scale the longitudinal coordinate (i.e., $X = x^*/L_e^*$). The values of the relevant dimensionless parameters adopted in the calculations are $\mathcal{K} = 0.16$, $\mathcal{K} = 0.$, $\mathcal{S} = 0.44$, $\mathcal{R} = 1.0$; $\epsilon = 0.24$, and $d_s = d_s^*/D_0^* = 1.11 \times 10^{-5}$. These values, for example, are achieved by considering an estuary 30 km long, with a constant width, an initial depth of 9.0 m, and a mean sediment grain diameter of 0.1 mm, forced by a semidiurnal tide with amplitude 2.2 m, characterized by a velocity scale $U_0^* = 0.6$ m s^{-1} and a Manning roughness coefficient of 0.0326 s $m^{-1/3}$.

de Swart [2000], displaying the presence of deep scours, inflection points, and the possibility of multiple solutions.

[36] Figure 2 shows a typical example of the bottom evolution from an initial flat bed configuration for the case of a strongly dissipative ($\mathcal{R}/\mathcal{S} = 2.9$), strongly convergent ($\mathcal{K} = 0.6$) estuary, with a relatively small ratio of tidal amplitude to flow depth ($\epsilon = 0.29$). It clearly appears that the sediments scoured in the seaward portion of the estuary are flushed toward the middle and inner reaches of the estuary, generating a sediment front which migrates landward. As the front reaches the inner (closed) end of the estuary, it is completely reflected, thus leading to the formation of a very shallow area in the inner portion of the estuary. The longitudinal extension of this area fixes the length of the estuary and eventually grows until a bottom profile forms, which ensures a vanishing net sediment flux all along the estuary and a nearly constant value of the maximum flood/ebb speed (see Figure 3a). Such a profile is characterized by an upward concavity and by a well-defined depth at the inlet section. This scenario is consistent with many field observations from both tidal estuaries and coastal

lagoon channels with a funnel shape [*Myrick and Leopold*, 1963; *Wallis and Knight*, 1984; *Speer et al.*, 1991; *French and Stoddart*, 1992; *Ayles and Lapointe*, 1996]. In Figure 3b we report the dimensionless tidal amplitude a and the phase lag ϕ between the maximum water surface elevation and the maximum flood speed as a function of the distance from the mouth. It clearly appears that in the portion of the estuary which never dries up, a tends to slightly increase landward, while ϕ keeps nearly constant, attaining the value $\pi/2$ typical of strongly dissipative, strongly convergent estuaries [see *Lanzoni and Seminara*, 1998]. On the contrary, in the inner reaches of the estuary, where the bottom dries during the low tide, both a and ϕ tend to decrease appreciably.

[37] It is important to note that the final bottom profile shown in Figure 2 must be regarded as a quasi-equilibrium configuration. Indeed, as it is shown in Figure 3c, as the bottom evolves, the net landward sediment flux associated with flood dominance progressively decreases. The rate of decreasing is relatively high in the initial stages of the morphological evolution, but it tends to vanish asymptotically as the equilibrium



(a) Maximum dimensionless flood/ebb flow speed (scaled with U_0^* , i.e., a typical value of the depth-averaged velocity within the estuary) and (b) dimensionless tidal amplitude a (scaled with the value of the flow depth at the outlet) and phase lag ϕ between the maximum tide elevation and the maximum flood flow speed plotted along the estuary for the final bottom configuration shown in Figure 4. The estuary length L_e^* has been used to scale the longitudinal coordinate (i.e., $X = x^*/L_e^*$). (c) Temporal evolution of the global dimensionless net sediment flux $Q_{s,tot}$ (i.e., tidally averaged, integrated all along the estuary, and scaled by $\sqrt{\Delta g d_s^{*3}}$) for the bottom evolution shown in Figure 4.

configuration is reached. The morphological changes associated with the landward flushing of sediments, in fact, lead to a progressive decrease of the tidal distortion and therefore of the net sediment flux conveyed. This mutual interplay between morphological changes and hydrodynamic field induces an

evolutionary trend in which the bottom modification rate decreases dramatically, thus implying that bottom equilibrium is only reached asymptotically.

[38] The effect of channel convergence is shown in Figures 4 and 5, where results of calculations carried out for an estuary similar to that of Figure 2 but with a constant width (i.e., $\mathcal{K} = 0$) are reported. It turns out that the picture outlined above does not change. However, in this case the bottom slope tends to attain a nearly constant value (Figure 4).

[39] It is hard to find data on the temporal evolution of the bed profile of real estuaries to fully substantiate the above scenario. However, some comparison can be made with the observed bottom profiles of fairly stable tidal channels, like those located in the northern part of the lagoon of Venice. The geometrical and hydrodynamic characteristics of four of these channels (i.e., Canale San Felice, Canale San Lorenzo, Canale Riga, Canale dei Bari) are reported in Table 1 along with the typical values of ϵ and of the ratios \mathcal{K}/\mathcal{F} and \mathcal{R}/S . Note that in order to calculate reliable values of the dimensionless parameters governing the flow dynamics we have estimated the velocity scale U_0^* (≈ 0.4 m/s) and the Manning bed Roughness coefficient m (≈ 0.0313 s/m^{1/3}) from both field measurements [Istituto di Idraulica dell'Università di Padova, 1979] and results of a two-dimensional hydrodynamic numerical model calibrated on the lagoon of Venice (A. Defina, personal communication, 2001). Results of our comparison are reported in Figure 6. In order to appreciate how satisfactory such comparison can be considered, the reader should note that the oscillations exhibited by the actual bottom profiles are due to various mesoscale processes, namely, meandering, the presence of junctions, and large-scale bed forms. Overall comparison seems to be fairly satisfactory.

[40] Obviously, the evolutionary scenario may appreciably change as a consequence of changes in the initial conditions or in the boundary conditions. For example, if the estuary is relatively short, it will be filled with sediments before an equilibrium profile (i.e., ensuring a vanishing net sediment flux) can be established. In other words, the shallow area which forms as a consequence of the front reflection will gradually extend to the entire estuary. Also, the presence of a nonnegligible flux of marine sediments at the estuary mouth may alter considerably the above picture. First of all, the fact that $\bar{q}_{s0} \neq 0$ implies that, at equilibrium, the condition of vanishing sediment flux at the landward boundary can never be fulfilled (see relationship (26)), hence the entire bottom profile tends to rise, and the estuary will fill progressively. Consequently, an equilibrium configuration can never be attained unless the mean sea level itself will increase at a suitable rate. However, it must be noticed that such an infilling process, often reinforced by the deposition of material transported by the river, favors the accretions of tidal flats and salt marshes. As the intertidal storage area exceeds a critical value, a transition from flood dominance to ebb dominance is likely to occur which might stop the net import of sediments inside the estuary and lead to a dynamically stable situation [Speer and Aubrey, 1985; van Dongeren and de Vriend, 1994].

[41] The latter arguments can be quantitatively confirmed by extending the present model such to cover the effects of sedi-

Table 1. Observed Geometric Properties and Dimensionless Parameters Characterizing Four Tidal Channels in the Venice Lagoon^a

Channel	D_0^* , m	L_0^* , m	L_b^* , m	C_0^*	ϵ	\mathcal{K}/\mathcal{F}	\mathcal{R}/S
S. Lorenzo	4.0	5375	4000	12.87	0.175	1.34	4.15
S. Felice	4.0	9872	4500	12.87	0.175	2.19	4.15
dei Bari	5.0	9826	6850	13.36	0.140	1.43	3.08
Riga	4.0	2668	6850	12.87	0.175	0.39	4.15

^aThe characteristic values of the amplitude a_0^* and of the angular frequency ω^* of the main component of the tidal wave within the lagoon are 0.7 m and 1.5×10^{-4} s⁻¹, respectively. A typical value of the depth-averaged velocity U_0^* in the channels is 0.4 m s⁻¹ [Istituto di Idraulica dell'Università di Padova, 1979]. Two-dimensional hydrodynamic numerical models calibrated on the Venice lagoon indicate that a typical value of the Manning bed roughness coefficient m is 0.0313 s m^{-1/3} (A. Defina, personal communication, 2001).

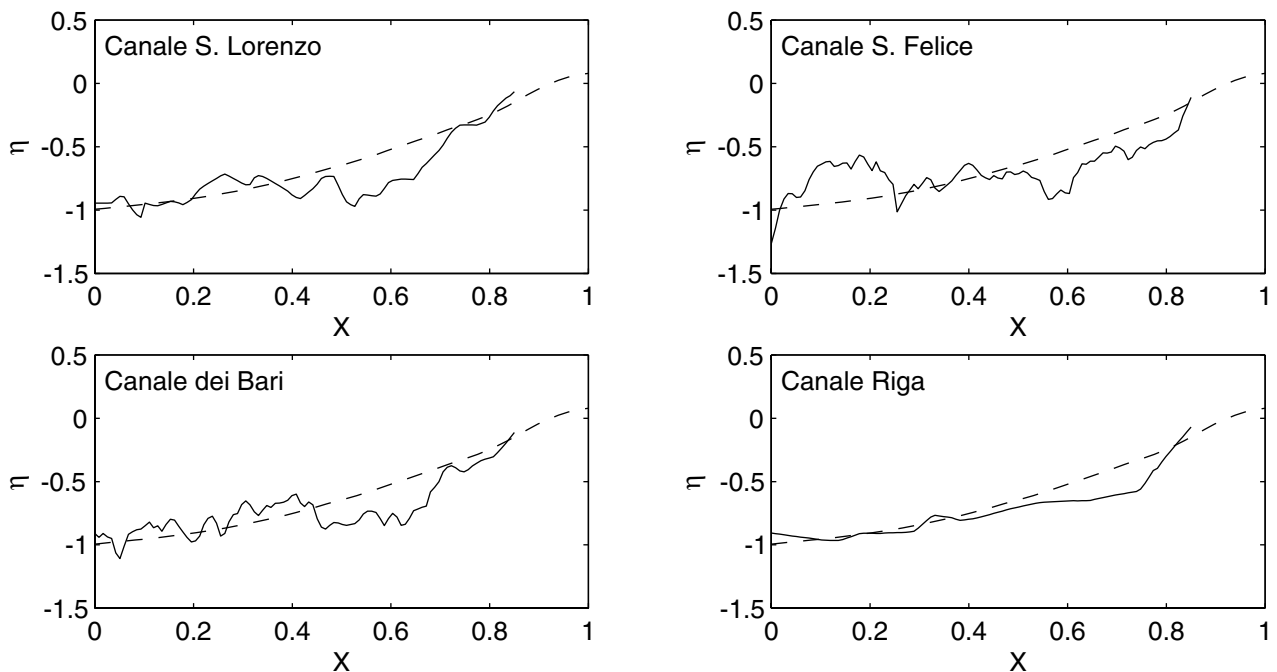


Figure 6. Observed bottom elevation along some stable tidal channels located in the lagoon of Venice (solid lines) compared with the equilibrium bed profile calculated by choosing the values of the relevant dimensionless parameters such that $\epsilon (= 0.2)$, $\mathcal{K}/\mathcal{F} (= 5.13)$, and $\mathcal{R}/\mathcal{S} (= 3.50)$ are qualitatively similar to the observed ones reported in Table 1 (dashed lines). The bed elevation at each cross section η is here scaled with the value of the flow depth at the outlet; the longitudinal coordinate X has been scaled with the channel length L_e^* . Note that the maximum value of X observed in each tidal channel is lower than 1 owing to the lack of data in the landward reaches, i.e., where the bottom elevation exceeds about -0.5 m above the mean sea level.

ment exchange between the main channel and the adjacent tidal flats and salt marshes. However, note that such an extension is not straightforward because of the role played by the cohesive nature of intertidal areas and by the vegetation growing on salt marshes.

[42] It is of great interest to analyze the profiles reported in Figures 2 and 4 to determine the relationship which, at a given section, relates the volume of water exchanged during one tidal cycle (i.e., the tidal prism) and the minimum cross-sectional flow area. It has long been recognized that a power law correlation between tidal prism P^* and inlet minimum cross-sectional area A_{\min}^* holds for a large number of systems believed to have achieved dynamic equilibrium [O'Brien, 1969; Jarrett, 1976]. More recently, Friedrichs [1995] and Rinaldo *et al.* [1999] found that a near proportionality of cross-sectional area and peak tidal discharge (which replaces the tidal prism) also exists for sheltered sections of several tidal systems. Friedrichs [1995] explains the existence of such a relationship by relating the equilibrium cross-sectional geometry to the so-called stability shear stress τ_s^* , i.e., the total bottom shear stress just necessary to maintain a zero along-channel gradient in net sediment transport. Analyzing 242 cross sections in 26 tidal systems, Friedrichs [1995] concludes that the upper bound of the equilibrium cross-sectional geometry of tidal channels is predicted by assuming as a lower bound on τ_s^* the critical grain shear stress for sediment motion (or, for muddy bottoms, the critical erosion shear stress). Our work shows that in absence of a net import of sediment either from the sea or from the river, equilibrium is achieved when the evolution of the bed profile has reached a condition such that the net sediment flux in a tidal cycle vanishes everywhere in the channel. Moreover, Figure 7 shows the minimum cross-sectional area as a function of the tidal prism for the bottom profile configurations of Figures 2 and 4. It clearly appears how a power law relationship is

progressively attained along the estuary as the bottom evolves toward a configuration allowing the equilibrium condition of vanishing net sediment flux everywhere. However, a break in the power law relationship appears to characterize the smaller cross-sectional areas in the inner portion of the estuary, where wetting and drying are likely to affect heavily the dynamic of sediment transport. A similar deviation from the power law relationship has been observed by Rinaldo *et al.* [1999] in their study of the empirical geomorphic relationship exhibited by the network of tidal channels draining the lagoon of Venice. Rinaldo *et al.* [1999] interpret such a departure from a power law as an artifact of the poor morphologic resolution of small channels in their model. However, the plot of the tidal prism versus the maximum cross-sectional area A_{\max} reported in Figure 8 gives, as suggested by one of the referees, a deviation of the power law relationship toward the opposite direction of Figure 7, thus indicating that the departure from linearity is indeed associated to wetting and drying.

[43] Finally, it is worthwhile to stress the fact that the major assumption employed in our model is the instantaneous adjustment of the sediment flux to the local transport capacity. In other words, we have neglected the phase lag required for such adjustment process. The latter assumption is particularly severe close to the slack water periods when equilibrium between entrainment and deposition cannot occur, as sediments simply settle in a quasi-quiet water body.

Appendix A

[44] Let us consider within the integration domain Ω a representative elementary area $A(X, Y)$, centered on the point

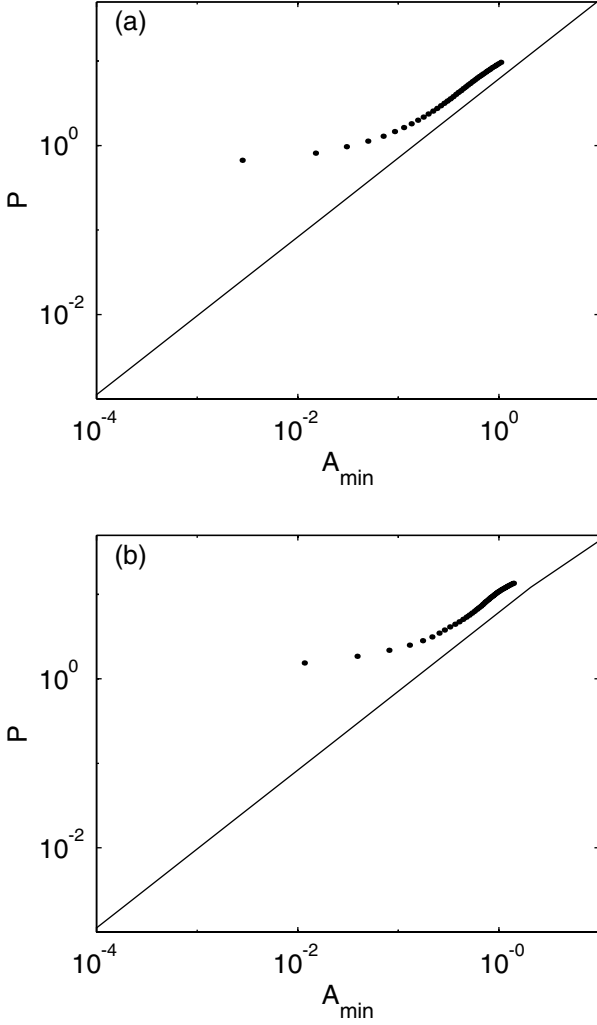


Figure 7. Dimensionless tidal prism ($2P^*\omega^*/D_0^*B_0^*U_0^*$) plotted versus the minimum dimensionless cross-sectional flow area ($A_{\min}^*/D_0^*B_0^*$) for the various sections along the estuary. (a) Strongly dissipative, strongly convergent estuary of Figure 2 and (b) strongly dissipative, constant-width estuary of Figure 4. The continuous line represents *Jarrett's* [1976] relationship.

(X, Y) , of size $O(L)$, where L is the length scale characterizing the computational elements used to discretize Ω (in the following, for simplicity, the star apex denoting dimensional qualities will be dropped). Moreover, let D_0 and e denote the average water depth and a characteristic scale of the spatial variations of the bed elevation over A , respectively. We are interested in deriving a set of depth-averaged, shallow water equations valid on the macroscopic scale L and suitable to treat partially dry areas, namely, situations in which D_0 and e are of the same order of magnitude. To this end the following phase function is introduced:

$$\psi(x, y, z) = \begin{cases} 1 & z > \eta \\ 0 & z \leq \eta, \end{cases} \quad (\text{A1})$$

where η is the local bottom elevation above a horizontal reference plane (x, y) and z is a vertical coordinate with the z axis directed upward. The function ψ depends only on the geometric configuration of the bottom and can be treated as a generalized function [Drew, 1983]; in particular, $\nabla\psi$ behaves as a delta function picking out the bottom surface. The phase average of a given function $f(x, y, z, t)$ can then be defined as

$$F(X, Y, z, t) = \frac{1}{A} \int_A f \psi dx dy, \quad (\text{A2})$$

where uppercase is used to denote phase-averaged variables representing average (macroscopic) properties of the representative elementary area A . Note that setting $f = 1$ yields

$$\Psi(X, Y, z) = \frac{1}{A} \int_A \psi(x, y, z) dx dy \quad (\text{A3})$$

that is the fraction of $A(X, Y)$ that becomes wetted when the free surface elevation H exceeds z . Indeed, if the length scale over which the water surface elevation varies is much larger than L , the water elevation H can be assumed to be constant over each representative elementary area, and the quantity

$$D = \int_{-\infty}^H \Psi dz \quad (\text{A4})$$

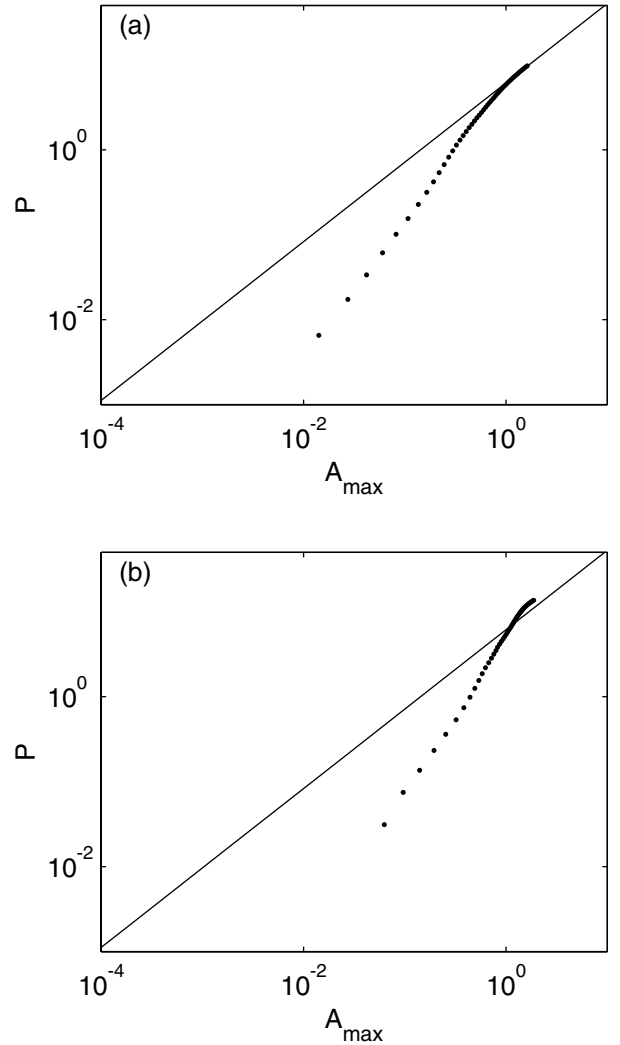


Figure 8. Dimensionless tidal prism ($2P^*\omega^*/D_0^*B_0^*U_0^*$) plotted versus the maximum dimensionless cross-sectional flow area ($A_{\max}^*/D_0^*B_0^*$) for the various sections along the estuary. (a) Strongly dissipative, strongly convergent estuary of Figure 2 and (b) strongly dissipative, constant-width estuary of Figure 4. The continuous line represents *Jarrett's* [1976] relationship.

is the water volume per unit area residing over A , which can be regarded as the effective flow depth characterizing the point (X, Y) .

[45] In order to derive the desired set of governing equations the above procedure is applied to the classical Reynolds equations in which the Boussinesq closure model is considered and, owing to the assumption of gradually varying flow conditions, the pressure is taken to be hydrostatically distributed along the vertical. The three momentum equations and the continuity equation are first multiplied by ψ and averaged over the elementary representative area A . The resulting equations are then integrated over the flow depth and suitably simplified by means of the phase-averaged kinematic and dynamic conditions at the boundaries. The details of the procedure are thoroughly described by Defina [2000]. For a one-dimensional flow field, the resulting dimensional momentum and continuity equations read

$$\Psi_H H_t + (BUD)_{,x} = 0 \quad (A5)$$

$$U_{,t} + UU_{,x} + gH_{,x} + \frac{U|U|}{C^2} \left(\frac{D}{\Phi}\right)^2 = 0, \quad (A6)$$

where the form of the functions $\Psi_H = \Psi(X, Y, H)$ and Φ strictly depends on the statistical distribution of bottom elevation within each representative elementary area. Under the assumption that, as a first approximation, the probability density function is Gaussian, the functions Ψ_H and Φ can be expressed analytically through the following relationships:

$$\Psi_H = \frac{1}{2} \operatorname{erf}(\xi_H); \quad \xi = -2\frac{z-\eta}{e}; \quad \xi_H = -2\frac{H-\eta}{e}; \quad (A7)$$

$$\Phi = \left\{ D + 0.27\sqrt{eD} \exp\left(-2\frac{D}{e}\right) \right\}^{3/2}, \quad (A8)$$

where $\operatorname{erf}(\xi) = 1 - \operatorname{erfc}(\xi)$, having denoted by erf the error function. It is easily recognized that the classical de Saint Venant equations are recovered when $D \gg e$ since $\Psi_H = 1$ and $\Phi = D^{3/2}$. Also, note that the equivalent flow depth given by (A4) becomes

$$D = \frac{e}{4} \int_{\xi_H}^{\infty} \operatorname{erfc}(\xi) d\xi = \frac{e}{4} \left[\frac{1}{\sqrt{\pi}} \exp(-\xi_H^2) - \xi_H \operatorname{erfc}(\xi_H) \right]. \quad (A9)$$

We now apply the outlined averaging procedure to derive the value of the Shields parameter associated to a generic representative elementary area. The local value of the Shields parameter reads

$$\theta(x, y, t) = \frac{|\tau|/\rho}{\Delta g d_s}, \quad (A10)$$

having denoted by τ the local shear stress acting at the bed interface. In this respect, let us note that the spatial variations of η are taken to be slow enough to approximate τ with the longitudinal component of the stress acting at the bed. Recalling the properties of the phase function ψ , in particular, noting that the z derivative of ψ is a delta distribution centered at $z = \eta$, we observe that in a gradually varying flow in which gravity is mainly balanced by friction τ can be satisfactorily approximated as follows:

$$\frac{|\tau|}{\rho} = g \frac{\partial H}{\partial x} \int_{-\infty}^H (H-z) \psi_{,z} dz = g \frac{U^2}{C^2} \left(\frac{D}{\Phi}\right)^2 \int_{-\infty}^H (H-z) \psi_{,z} dz. \quad (A11)$$

Hence the averaged value of the Shields parameter over the representative elementary area $A(\Theta)$ is easily found to be

$$\theta = \frac{1}{A} \int_A \frac{|\tau|/\rho}{\Delta g d_s} dx dy = \frac{1}{\Delta g d_s} \frac{DU^2}{C^2} \left(\frac{D}{\Phi}\right)^2. \quad (A12)$$

This value of the Shields parameter can then be substituted into (16) and (21) to evaluate the bed load and suspended load associated with each representative elementary area A .

[46] **Acknowledgments.** This work has been developed within the framework of the National Project supported by the Italian Ministry of University and Scientific Research Cofin 1997 Morfodinamica Fluviale e Costiera and was completed within the context of the research projects Idrodinamica e Morfodinamica di Ambienti a Marea, supported by the Italian Ministry of University, and Analisi e Monitoraggio dei Processi Morfologici nel Sistema Lagunare Veneziano, funded by Corila. We thank C. T. Friedrichs and an anonymous reviewer for their constructive criticism on the draft of this paper.

References

- Abbott, M. B., Continuous flows, discontinuous flows and numerical analysis, *J. Hydraul. Res.*, 12, 417–467, 1974.
- Allen, G. P., J. C. Salomon, P. Bassoullet, Y. Du Penhoat, and C. De Grandpré, Effects of tides on mixing and suspended sediment transport in macro tidal estuaries, *Sediment. Geol.*, 26, 69–90, 1980.
- Ayles, C. P., and M. F. Lapointe, Downvalley gradients in flow patterns, sediment transport and channel morphology in a small macrotidal estuary: Dipper Harbour Creek, New Brunswick, Canada, *Earth Surf. Processes Landforms*, 21, 829–842, 1996.
- Bagnold, R. A., An approach to the sediment transport problem for general physics, *Prof. Pap. 422-I*, U.S. Geol. Surv., Washington, D. C., 1966.
- Bates, P. D., and J. M. Hervouet, A new method for moving boundary hydrodynamic problems in shallow water, *Proc. R. Soc. London, Ser. A*, 455, 3107–3128, 1999.
- Bhalla, S. M., and M. H. Chaudhry, Numerical modelling of aggradation and degradation in alluvial channels, *J. Hydraul. Eng.*, 117, 1145–1164, 1991.
- Boon, J. D., and R. J. Byrne, On basin hypsometry and the morphodynamic response of coastal inlet systems, *Mar. Geol.*, 40, 27–48, 1981.
- Cunge, J. A., F. M. Holly, and A. Verwey, *Practical Aspects of Computational River Hydraulics*, 420 pp., Pitman, London, 1980.
- Dalrymple, R. W., and R. M. Rhodes, Estuarine dunes and bars, in *Geomorphology and Sedimentology of Estuaries*, Dev. Sedimentol., 53 pp., Elsevier Sci., New York, 1995.
- Dalrymple, R. W., B. A. Zaitlin, and R. Boyd, Estuarine facies models: Conceptual basis and stratigraphic implications, *J. Sediment. Petrol.*, 62, 1130–1146, 1992.
- Defina, A., Two-dimensional shallow flow equations for partially dry areas, *Water Resour. Res.*, 36, 3251–3264, 2000.
- Defina, A., L. D'Alpaos, and B. Maticchio, A new set of equations for very shallow water and partially dry areas suitable to 2D numerical models, in *Proceedings of the Specialty Conference on Modelling of Flood Propagation Over Initially Dry Areas*, edited by P. Molinaro, and L. Natale, pp. 72–81, Milan, Italy, 1994.
- Drew, D. A., Mathematical modeling of two-phase flow, *Annu. Rev. Fluid Mech.*, 15, 261–291, 1983.
- Dronkers, J., Tidal asymmetry and estuarine morphology, *Neth. J. Sea Res.*, 20, 117–131, 1986.
- Dyer, K. R. X., Sediment transport processes in Estuaries, in *Geomorphology and Sedimentology of Estuaries*, edited by G. M. E. Perillo, pp. 423–449, Elsevier Sci., New York, 1995.
- Engelund, F., A criterion for the occurrence of suspended load, *Houille Blanche*, 8, 7, 1965.
- Engelund, F., and E. Hansen, *A Monograph on Sediment Transport in Alluvial Streams*, Danish Tech. Press, Copenhagen, 1967.
- Exner, F. M., Über die wechselwirkung zwischen wasser und geschiebe in flüssen, *Sitzungber. Acad. Wissenschaften Wien Math. Naturwiss. Abt. 2a*, 134, 165–180, 1925.
- French, J. R., and D. R. Stoddart, Hydrodynamics of saltmarsh creek systems: Implication for morphologic development and material exchange, *Earth Surf. Processes Landforms*, 17, 235–252, 1992.
- Friedrichs, C. T., Stability, shear stress and equilibrium cross-sectional geometry of sheltered tidal channels, *J. Coastal Res.*, 4, 1062–1074, 1995.
- Friedrichs, C. T., and D. G. Aubrey, Nonlinear tidal distortion in shallow

- weel-mixed estuaries: A synthesis, *Estuarine Coastal Shelf Sci.*, 26, 521–545, 1988.
- Friedrichs, C. T., B. D. Armbrust, and H. E. de Swart, Hydrodynamics and equilibrium sediment dynamics of shallow funnel-shaped tidal estuaries, in *Physics of Estuaries and Coastal Seas*, edited by J. Dronkers, A. A. Balkema, Brookfield, Vt., 1998.
- Galappatti, R., A depth integrated model for suspended transport, *Commun. Hydraul. Rep.* 83–7, Delft Univ. of Technol., Netherlands, 1983.
- Galappatti, R., and C. B. Vreugdenhil, A depth integrated model for suspended transport, *J. Hydraul. Res.*, 23, 1985.
- Garcia-Navarro, P., and J. M. Saviron, McCormack's method for the numerical simulation of one-dimensional discontinuous open channel flow, *J. Hydraul. Res.*, 30, 95–105, 1992.
- Goud, M. R., and D. G. Aubrey, Theoretical and observational estimates of nearshore bedload transport rates, *Mar. Geol.*, 64, 91–111, 1985.
- Groen, P., On the residual transport of suspended matter by an alternating tidal current, *Neth. J. Sea Res.*, 3, 564–574, 1967.
- Hirsch, C., *Numerical Computation of Internal and External Flows*, vol. 1, John Wiley, New York, 1990a.
- Hirsch, C., *Numerical Computation of Internal and External Flows*, vol. 2, John Wiley, New York, 1990b.
- Istituto di Idraulica dell'Università di Padova, Le correnti di marea nella Laguna di Venezia, technical report, 95 pp., Com. per lo studio dei provvedimenti a difesa della città di Venezia ed a salvaguardia dei suoi caratteri ambientali, Minist. dei Lavori Pubbl., Padua, Italy, 1979.
- Jarrett, J. T., Tidal prism-inlet area relationship, *Gen. Invest. Tidal Inlets, Rep.* 3, U.S. Army Corps Coastal Eng. Res. Center, Vicksburg, Miss., 32 pp., 1976.
- Jay, D. A., Green's law revisited: Tidal long-wave propagation in channels with strong topography, *J. Geophys. Res.*, 96, 20,585–20,598, 1991.
- Lanzoni, S., and G. Seminara, On tide propagation in convergent estuaries, *J. Geophys. Res.*, 103, 30,793–30,812, 1998.
- Lyn, D. A., Unsteady sediment transport modelling, *J. Hydraul. Eng.*, 113(1), 1–15, 1987.
- Lyn, D. A., and P. Goodwin, Stability of a general Preissmann scheme, *J. Hydr. Eng.*, 113(1), 16–28, 1987.
- Meyer-Peter, E., and R. Müller, Formulas for bedload transport, paper presented at 2nd Congress, Int. Assoc. of Hydraul. Res., Stockholm, Sweden, 1948.
- Myrick, R. M., and L. B. Leopold, Hydraulic geometry of a small tidal estuary, *U.S. Geol. Surv. Prof. Pap.*, 422-B, 18 pp., 1963.
- Nichols, M. N., Sediment accumulation rates and relative sea-level rise in lagoons, *Mar. Geol.*, 88, 201–219, 1989.
- Nichols, M. N., and J. D. Boon, Sediment transport processes in coastal lagoons, in *Coastal Lagoon Processes, Oceanogr. Ser.*, vol. 60, edited by B. Kjerfve, pp. 157–211, Elsevier Sci., New York, 1994.
- Niño, Y., and M. Garcia, Experiments on particle-turbulence interactions in the near-wall region of an open channel flow: Implications for sediment transport, *J. Fluid Mech.*, 326, 285–319, 1996.
- O'Brien, M. P., Equilibrium flow areas of inlets on sandy coasts, *J. Waterw. Harbors Coastal Eng. Div. Am. Soc. Civ. Eng.*, 95, 43–52, 1969.
- Officer, C. B., Physical dynamics of estuarine suspended sediments, *Mar. Geol.*, 40, 1–14, 1981.
- Parker, B. B., The relative importance of the various nonlinear mechanisms in a wide range of tidal interactions, in *Tidal Hydrodynamics*, edited by B. B. Parker, pp. 237–268, John Wiley, New York, 1991.
- Perillo, G. M. E., Geomorphology and sedimentology of estuaries: An introduction, in *Geomorphology and Sedimentology of Estuaries*, edited by G. M. E. Perillo, pp. 1–16, Elsevier Sci., New York, 1995.
- Postma, H., Sediment transport and sedimentation in the estuarine environment, in *Estuaries, Am. Ass. Adv. Sci.*, vol. 83, edited by G. H. Lauff, pp. 158–179, Washington, D. C., 1961.
- Rinaldo, A., S. Fagherazzi, S. Lanzoni, M. Marani, and W. E. Dietrich, Tidal networks, 3, Landscape-forming discharges and studies in empirical geomorphic relationship, *Water Resour. Res.*, 35, 3919–3929, 1999.
- Rouse, H., Modern conceptions of the mechanics of turbulence, *Trans. Am. Soc. Civ. Eng.*, 102, 463–543, 1937.
- Schuttelaars, H. M., and H. E. de Swart, An idealized long-term morphodynamic model of a tidal embayment, *Eur. J. Mech. B Fluids*, 15, 55–80, 1996.
- Schuttelaars, H. M., and H. E. de Swart, Initial formation of channels and shoals in a short tidal embayment, *J. Fluid Mech.*, 386, 15–42, 1999.
- Schuttelaars, H. M., and H. E. de Swart, Multiple morphodynamic equilibria in tidal embayment, *J. Geoph. Res.*, 105, 24,105–24,118, 2000.
- Shetye, S. R. G., and A. D. Gouveya, On the role of geometry of cross-section in generating flood dominance in shallow estuaries, *Estuarine Coastal Shelf Sci.*, 35, 113–126, 1992.
- Speer, P. E., and D. G. Aubrey, A study on non-linear tidal propagation in shallow inlet/estuarine systems, part II, Theory, *Estuarine Coastal Shelf Sci.*, 21, 206–240, 1985.
- Speer, P. E., D. G. Aubrey, and C. Friedrichs, Nonlinear hydrodynamics of shallow tidal inlet/bay systems, in *Tidal Hydrodynamics*, edited by B. B. Parker, pp. 321–339, John Wiley, New York, 1991.
- Stevenson, J. C., L. G. Ward, and M. S. Kearney, Vertical accretion in marshes with varying rates of sea level rise, in *Estuarine Variability*, edited by D. A. Wolfe, pp. 241–259, Academic, San Diego, Calif., 1986.
- Sumer, B. M., and R. Deigaard, Particle motions near the bottom in turbulent flow in an open channel, part 2, *J. Fluid Mech.*, 109, 311–339, 1981.
- van Dongeren, A. R., and H. J. de Vriend, A model for morphological behaviour of tidal basins, *Coastal Eng.*, 22, 287–310, 1994.
- van Rijn, L. C., Sediment transport, part I, Bedload transport, *J. Hydraul. Eng.*, 110, 1431–1456, 1984a.
- van Rijn, L. C., Sediment transport, part II, Suspended load transport, *J. Hydraul. Eng.*, 110, 1613–1641, 1984b.
- van Rijn, L. C., Sediment transport, part III, Bed forms and alluvial roughness, *J. Hydraul. Eng.*, 110, 1733–1754, 1984c.
- van Rijn, L. C., Handbook of sediment transport by current and waves, *Rep. H 461*, Delft Hydraul., Delft, Netherlands, 1990.
- Wallis, S. G., and D. W. Knight, Calibration studies concerning a one-dimensional numerical tidal model with reference to resistance coefficients, *Estuarine Coastal Shelf Sci.*, 19, 541–562, 1984.
- Wells, J. T., Tide dominated estuaries and tidal rivers, in *Geomorphology and Sedimentology of Estuaries*, edited by G. M. E. Perillo, pp. 179–205, Elsevier Sci., New York, 1995.

S. Lanzoni, Dipartimento di Ingegneria Idraulica, Marittima e Geotecnica, Università di Padova, via Loredan 20, I-35131 Padova, Italy. (lanzo@idra.unipd.it)

G. Seminara, Dipartimento di Ingegneria Ambientale, Università di Genova, via Montalegno 1, 45100 Genova, Italy. (sem@idra.unige.it)